




Article

The importance of cation–cation repulsion in the zircon–reidite phase transition and radiation-damaged zircon

Makoto Tokuda^{1,2*} , Akira Yoshiasa^{1,2}, Hiroshi Kojitani³, Saki Hashimoto³, Seiichiro Uehara⁴, Tsutomu Mashimo¹, Tsubasa Tobase² and Masaki Akaogi³

¹Institute of Pulsed Power Science, Kumamoto University, Kurokami 2-39-1, Kumamoto, 860-8555, Japan; ²Graduate School of Science and Technology, Kumamoto University, Kurokami 2-39-1, Kumamoto, 860-8555, Japan; ³Department of Chemistry, Gakushuin University, Mejiro, Toshima-ku, Tokyo, 171-8588, Japan; and ⁴Department of Earth and Planetary Sciences, Faculty of Science, Kyushu University, Hakozaki, Fukuoka, 812, Japan

Abstract

Single crystals of synthetic reidite and natural radiation-damaged zircon from Okueyama, Japan were investigated using X-ray diffraction. The pressure-induced zircon–reidite transition is described by the twisting and translations of SiO₄ tetrahedra with disappearance of the SiO₄–ZrO₈ shared edges. The lattice of radiation-damaged zircons expands mainly from α -decays of radioactive elements such as U and Th. Although old radiation-damaged zircons show anomalous lattice distortion, young radiation-damaged zircons do not show such distortions. These distortions are caused by thermal recovery that suppresses the Si⁴⁺–Zr⁴⁺ repulsion between the SiO₄ tetrahedron and ZrO₈ dodecahedron. These changes in structure can be understood by considering the cation–cation repulsion between the SiO₄–ZrO₈ shared edges.

Keywords: reidite, zircon, phase transition, radiation damage, cation–cation repulsion

(Received 18 August 2018; accepted 28 March 2019; Accepted Manuscript online: 22 May 2019; Associate Editor: Michael Rumsey)

Introduction

Ionic radii have been used widely to study and evaluate the crystal structure of compounds. Although ionic radius is a powerful tool for describing such structures, other factors should also be considered when discussing structural stability. Cation–cation repulsion comes into play when evaluating anisotropic lattice distortions in structures with edge-shared polyhedra, which cannot be predicted by ionic radii consideration alone. For instance, understanding the stability of the garnet structure requires studying the repulsion between cations across shared edges of polyhedra (Nakatsuka *et al.*, 1995, Tokuda *et al.*, 2018). In the structural study of the Y₃Al_{3–x}Ga_xO₁₂ (0 ≤ x ≤ 5) garnet solid solution, which shows a large deviation from Vegard's law, the preference of Ga³⁺ for the tetrahedral site brings about a decrease in the cation–cation repulsive force across the polyhedral shared edges with increasing Ga³⁺ content. The anomalous cation distribution in Y₃Al_{3–x}Ga_xO₁₂ garnet is a consequence of the strong covalency of the Ga–O bond and the need for decreased cation–cation repulsion (Nakatsuka *et al.* 1999).

In the ABO₄ zircon-type structure, a chain of alternating edge-sharing BO₄ tetrahedra and AO₈ triangular dodecahedra along the *c* axis is the principal structural unit. Similar chains of edge-sharing polyhedra exist in garnet-type structures. Fukunaga and Yamaoka (1979) investigated the pressure-induced phase transition

in ABX₄ type compounds and proposed the classification diagram of ABX₄ type compounds with two parameters $t = (r_A + r_B)/r_O$ and $k = r_A/r_B$, where *r* is the ionic radius of the respective element. In recent years, Errandonea and Manjón (2008) reviewed studies on pressure-induced phase transitions of ABX₄ compounds to understand the effect of pressure on their structure and physical properties on the basis of ionic radii. According to these studies, zircon ZrSiO₄ is transformed to scheelite-type ZrSiO₄ (reidite) by applying pressure. As well as the garnet structure, an investigation of the zircon–reidite transition from the viewpoint of cation–cation repulsion between shared edges of polyhedra will elucidate new aspects of the pressure-induced phase transition of ABX₄ compounds.

Recently, the high-pressure phase ZrSiO₄ (reidite) was discovered in an upper-Eocene impact ejecta layer in marine sediments on the upper continental slope of New Jersey, USA and on Barbados (Glass and Liu, 2001). Shock experiments showed that the phase transition from zircon to reidite started at a pressure of ~30 GPa and finished at ~53 GPa, at a temperature of ~600 K (Mashimo *et al.*, 1983; Kusaba *et al.*, 1985). The zircon–reidite transition and dissociation boundary were determined for pressures between 8.3–9.7 GPa and temperatures between 1100–1900 K by Ono *et al.* (2004) and Tange and Takahashi (2004), respectively. Akaogi *et al.* (2018) suggested that zircon transforms to reidite and dissociates into two phases (SiO₂ stishovite and cotunnite-type ZrO₂) at 330 km and 610 km depths, respectively, along the normal mantle geotherm. Reidite was first synthesised by Reid and Ringwood (1969). Then Liu (1979) revealed that reidite undergoes dissociation into an assemblage of SiO₂ stishovite and cotunnite-type ZrO₂ by using the static pressure range of

*Author for correspondence: Makoto Tokuda, Email: tokuda@imr.tohoku.ac.jp

Cite this article: Tokuda M., Yoshiasa A., Kojitani H., Hashimoto S., Uehara S., Mashimo T., Tobase T. and Akaogi M. (2019) The importance of cation–cation repulsion in the zircon–reidite phase transition and radiation-damaged zircon. *Mineralogical Magazine* 83, 561–567. <https://doi.org/10.1180/mgm.2019.27>

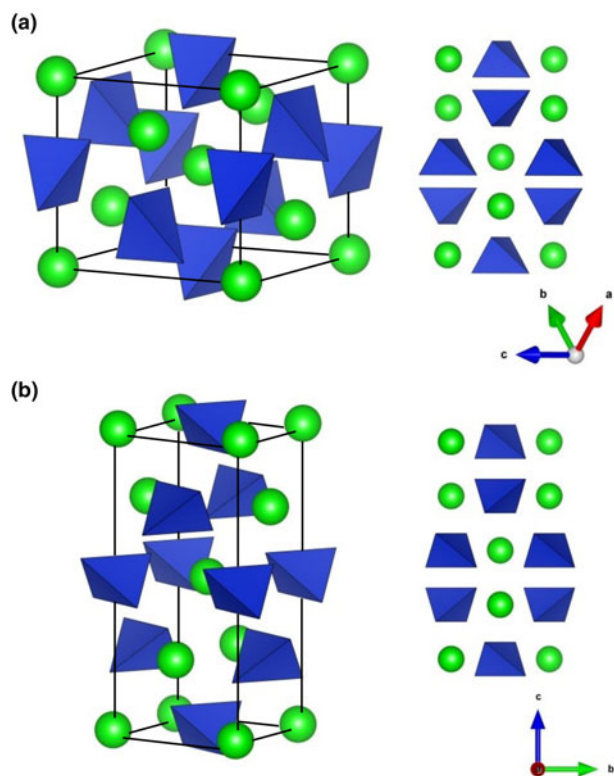


Fig. 1. Crystal structure of (a) zircon (Kolesov *et al.*, 2001) and (b) reidite. Circles and tetrahedra represent Zr^{4+} and SiO_4 , respectively (drawn using VESTA; Momma and Izumi, 2008).

10–30 GPa at $\sim 1000^\circ\text{C}$ with a diamond-anvil cell. Kusaba *et al.* (1986) reported that a zircon (space group $I4_1/amd$) from a recovered shock-compression sample converted to an isomorphous scheelite-type structure (space group $I4_1/a$), as shown in Fig. 1. Very limited reidite data are available, and structural investigations are reported only for powder X-ray diffraction.

Zircon ($ZrSiO_4$) has been used to determine the ages of tectonic events using host minerals for radioactive elements such as U or Th. Thus, radiation damaged (metamictised) zircons are often found in crustal igneous, metamorphic and sedimentary rocks. Metamictisation is defined as the amorphous state of a substance that has lost its periodic structure (Brøgger, 1893). Metamictisation is a radiation-induced, periodic-to-a-periodic phase transition caused by α -particles from the U or Th decay series (Hamberg, 1914). Damage by α -decay has two components that occur simultaneously. The first is that an α -particle (4.5–5.0 MeV) from a radionuclide displaces several hundred atoms, creating isolated Frenkel defect pairs at the end of its flight. The second is that an α -recoil atom (0.07–0.09 MeV) also generates Frenkel defect pairs and produces several thousand atomic displacements by releasing its energy to elastic scatterings. Anomalous distortion of lattice parameters has been reported for zircon from Sri Lanka. Murakami *et al.* (1991) suggested that point defects in the early stages of damage accumulation ($< 3.0 \times 10^{15}$ α -decays/mg) undergo self-annealing in natural zircon under ambient conditions.

We first report single-crystal data of synthetic scheelite-type $ZrSiO_4$ (reidite) and discuss its structural features compared with those in a previous report on synthetic zircon. Moreover, we report the structural refinement of a radiation-damaged

Table 1. Averaged chemical composition of Okueyama and Sri Lankan zircons (Ríos *et al.*, 2000)*.

	Okueyama zircon		Sri Lankan zircon	
	Content (wt.%)	Apfu	Content (wt.%)	Apfu
Si	14.96(10)	0.98(1)	14.54(2)	0.951(1)
Zr	49.39(76)	0.99(2)	49.2(2)	0.990(4)
Hf	1.75(23)	0.02(1)	1.30(3)	0.013(3)
U	1.34(18)	0.009(1)	0.11(1)	0.0010(1)
O	34.93	–	34.85	–
Total	102.37		100	

*Apfu – atoms per formula unit on the basis of O = 4.00 apfu.

natural zircon we obtained recently from Okueyama, Japan. This natural zircon is younger than that studied by Ríos *et al.* (2000) from Sri Lanka and shows no anomalous lattice distortion. Therefore, a structural comparison between the Sri Lankan and Okueyama zircons provides important information on the effect of radiation damage and its thermal recovery. In this study, we consider the zircon–reidite phase transition and the effect of radiation damage on zircon from the viewpoint of cation–cation repulsion between shared edges of polyhedra.

Experimental methods

Specimen preparation and characterisation

Zircon was synthesised from an equimolar mixture of reagent-grade ZrO_2 (>99%, Wako Co.) and SiO_2 (>99%, Kanto Kagaku Co.) by heating at 1773 K for 314 hr with nine times intermittent mixing. Reidite was synthesised from synthesised zircon using a Kawai-type double-staged multianvil apparatus at Gakushuin University. The starting material was put into a cylindrical Pt capsule heater in a 5 wt.% Cr_2O_3 -doped MgO octahedron, and was kept at 15 GPa and 1773 K for 3 h. After quenching under pressure, the sample was recovered to ambient conditions. The synthesised sample was confirmed as single-phase reidite by microfocus X-ray diffraction and powder X-ray diffraction.

Natural zircon crystals were obtained from granite in Okueyama, Miyazaki Prefecture, Japan, and are light yellow under sunlight and fluorescent yellow under ultraviolet light. The Okueyama granite is part of the Miocene pluton of the Outer Zone of Southwest Japan, and has been aged radiometrically at 14 Ma (Shibata, 1978). The compositions of the samples were determined with a JEOL scanning electron microscope (SEM JSM-7001F) and an Oxford energy dispersive X-ray analyser (EDS INCA SYSTEM). The composition of the Okueyama zircons is shown in Table 1. Wollastonite $CaSiO_3$, and pure metals of Zr, Hf and U were used as standard materials. The average content (ten spot analyses) totals ~ 102 wt.%. The Okueyama zircon contains 1.75(23) wt.% Hf and 1.34(18) wt.% U at the A site and no impurities at the B site. According to this result, the averaged chemical formula of the Okueyama zircon is $(Zr_{0.97}Hf_{0.02}U_{0.01})_{\Sigma 1.00}Si_{0.98}O_4$, with a somewhat low B-site total of 0.98(1) Si per formula unit. Lower B-site and excess A-site cations in the Okueyama zircon are also observed in Sri Lankan zircons (Murakami *et al.*, 1991).

Single-crystal X-ray diffraction

Single-crystal X-ray diffraction for the synthetic reidite and natural Okueyama zircon was performed using a SuperNova, Single source

Table 2. Crystal structure and single-crystal X-ray diffraction data for reidite and Okueyama zircon.

	Reidite	Okueyama zircon
Crystal data		
Chemical formula	ZrSiO ₄	Zr _{0.97} Hf _{0.02} U _{0.01} Si _{0.98} O ₄
Formula weight	183.31	183.31
Space group	I4 ₁ /a (No. 88)	I4 ₁ /amd (No. 141)
<i>a</i> (Å)	4.7309(1)	6.64292(18)
<i>c</i> (Å)	10.4799(4)	6.0139(2)
<i>V</i> (Å ³)	234.56(1)	265.38(2)
Density	5.191	4.712
<i>Z</i>	4	4
<i>F</i> ₍₀₀₀₎	344	344
Radiation, wavelength (Å)	MoKα, 0.71069	MoKα, 0.71069
μ (mm ⁻¹)	4.963	5.582
Crystal size (mm)	0.042 × 0.032 × 0.024	0.105 × 0.086 × 0.083
Data collection		
Diffractometer	Rigaku SuperNova Single source diffractometer with an HyPix3000 area detector	
Temperature (K)	293	293
Absorption correction	Gaussian	Gaussian
<i>T</i> _{min} , <i>T</i> _{max}	0.886, 0.927	0.738, 0.843
2θ range (°)	9.45 ≤ 2θ ≤ 90	9.14 ≤ 2θ ≤ 80
No. of measured, independent and observed [<i>I</i> > 2σ(<i>I</i>)] reflections	1970, 488, 436	1962, 233, 225
<i>R</i> _{int}	0.0176	0.0231
Refinement		
<i>R</i> ₁ [<i>F</i> ² > σ ² (<i>F</i> ²)], <i>wR</i> (<i>F</i> ²)	0.0156, 0.0409	0.0235, 0.0600
GoF	1.091	0.811
No. of parameters	14	13
Weighting scheme*	<i>a</i> = 0.0214; <i>b</i> = 0.0349	<i>a</i> = 0.0690; <i>b</i> = 0
Δ <i>p</i> _{max} , Δ <i>p</i> _{min} (e ⁻ Å ⁻³)	0.606, -0.866	1.515, -1.998

$$*w = 1/[\sigma^2(F_o^2) + (aP)^2 + bP]; P = (\text{Max}(F_o^2, 0) + 2F_c^2)/3$$

at offset/far, HyPix3000 diffractometer. Monochromated MoKα radiation obtained by an X-ray generator (50 kV and 0.8 mA) was focused by a mirror. Details of the data collection are listed in Table 2.

Refinement

The structure was obtained with the *ShelXT* solution program using intrinsic phasing and refined with the *ShelXL* refinement package using least-squares minimisation (Sheldrick, 2015). During the least-square refinements a correction for isotropic extinction was applied. After several refinement cycles the displacement parameters were converted from an isotropic to an anisotropic model. The refined coordination and atomic displacement parameters are listed in Table 3. The final *R*₁ factors of reidite and zircon were 0.0156 and 0.0235, respectively.

Results and discussion

Pressure-induced phase transition from zircon to reidite

Generally, pressure-induced phase transitions occur with increasing cation coordination number. However, an increase of cation coordination number is not sufficient to explain high-pressure transformation in *ABO*₄ compounds. Monazite-type arsenates and vanadates, for example, are known to transform to a scheelite-type structure under high pressure with no change of cation coordination number (Stubican and Roy, 1959). As for the zircon–reidite phase transition, the cation coordination

number does not change. The density of reidite increases ~10% from that of low-pressure-phase zircon. This compression was explained by Kusaba *et al.* (1986). The [110] direction in the zircon structure is converted by simple shearing to the [001] direction in the scheelite structure, during which the intersecting angle between [100] and [010] increases from 90° to ~115°, which causes the increase in ZrSiO₄ density. This mechanism accounts for structural transformation without long-range atomic diffusion. Hence, the *c* axis of the scheelite structure in reidite corresponds to the [110] direction of the zircon structure, as shown in Fig. 1. The respective vectors *a*_z, *b*_z and *c*_z can be represented by a linear combination with the vectors *a*_r, *b*_r and *c*_r in zircon:

$$\begin{aligned} a_z &= \cos 53.4^\circ a_r + \cos 67.6^\circ b_r + \cos 45^\circ c_r \\ b_z &= \cos 126.7^\circ a_r + \cos 112.4^\circ b_r + \cos 45^\circ c_r \\ c_z &= \cos 57.4^\circ a_r + \cos 147.4^\circ b_r + \cos 90^\circ c_r \end{aligned} \quad (1)$$

where *a*_z, *b*_z and *c*_z correspond to reidite axes and *a*_r, *b*_r and *c*_r to zircon axes. In the discussion of the zircon and reidite structures, attention should be given to the above correspondence of axes.

The configuration of SiO₄ tetrahedra is important in understanding the phase transition from zircon to reidite. A comparison of SiO₄ configurations between zircon and reidite is shown in Fig. 2. The zircon–reidite phase transition can be understood by twisting and translations of SiO₄ tetrahedra. From the view of the *a*_r axis in reidite (Fig. 2a), there is no tetrahedral displacement along the *b*_r axis. The SiO₄ translations are along the *a*_r and *c*_r axes. The large expansion (~12%) along the *c*_r axis is caused, however, by the large contraction (~17%) along the *a*_r axis observed from the view of the *b*_r axis.

The twisting and translations of SiO₄ tetrahedra in the zircon structure cause the shared edge between SiO₄ tetrahedra and ZrO₈ dodecahedra to disappear, as shown in Fig. 3. The disappearance of the SiO₄–ZrO₈ shared edge yields structural stability according to Pauling's third rule (Pauling, 1929, 1960). Although the density of reidite is higher than that of zircon, the volume of the SiO₄ tetrahedron of reidite is larger than that of zircon. The O–O atomic distances of SiO₄ also change in the phase transition. In the zircon structure, there are four larger O–O distances and two shorter O–O distances corresponding to the SiO₄–ZrO₈ shared edge. However, there are four shorter O–O distances and two longer ones in the reidite structure (Table 4). Such changes in O–O distance are caused by twisting of the SiO₄ tetrahedra. The SiO₄ twisting is represented by the rotation of O1–O2 and O3–O4 bonds perpendicular to the *a*_r axis, as shown in Fig. 3. The O1–O3 and O2–O4 distances in reidite expand as the SiO₄–ZrO₈ shared edge disappears. Although the mean-square displacement (MSD) of the Si atom in pure zircon is nearly isotropic despite the SiO₄–ZrO₈ shared edge, the MSD of the Si atom in reidite is anisotropic (*U*¹¹ < *U*³³). The thermal vibration ellipsoid of reidite Si is elongated only towards the longer O1–O2 and O3–O4 bonds in the tetrahedron. Because of the SiO₄ twisting, the 4₁ axis in zircon, which is the *c*_z axis, disappears, and the new 4₁ axis is generated as a primary axis along [110]_z, which corresponds to the *c*_r axis.

Although the SiO₄–ZrO₈ shared edges disappear, the ZrO₈–ZrO₈ shared edges remain through the phase transition. The ZrO₈–ZrO₈ shared-edge length in reidite is longer than that in zircon despite the closer Zr–Zr distance. As far as Zr⁴⁺–Zr⁴⁺ repulsion between ZrO₈–ZrO₈, this cation–cation repulsion contributes a structural destabilisation energetically. We can deduce

Table 3. Atom coordinates and refined anisotropic displacement parameters (\AA^2) for reidite, Okueyama zircon and previous reports.*

Sites	Atoms	Occupancy	x	y	z	U_{eq}	U^{11}	U^{22}	U^{33}	U^{12}	U^{13}	U^{23}
Reidite ($I4_1/a$)												
A (4b)	Zr	1.00	0	$\frac{1}{4}$	$\frac{5}{8}$	0.00397(5)	0.00414(6)	0.00414	0.00362(7)	0.0000	0.0000	0.0000
B (4a)	Si	1.00	0	$\frac{1}{4}$	$\frac{1}{8}$	0.00388(8)	0.00368(12)	0.00368	0.00427(17)	0.0000	0.0000	0.0000
O (16f)	O	1.00	0.25906(14)	0.09347(13)	0.04720(6)	0.00554(9)	0.0057(2)	0.0053(2)	0.00563(18)	0.00563(2)	0.00106(2)	-0.00050(2)
Okueyama zircon ($I4_1/amd$)												
A (4a)	Zr	0.97 (fix)	0	$\frac{3}{4}$	$\frac{1}{8}$	0.00870(9)	0.00912(10)	0.00912	0.00787(13)	0.0000	0.0000	0.0000
	Hf	0.02 (fix)										
	U	0.01 (fix)										
B (4b)	Si	0.98 (fix)	0	$\frac{3}{4}$	$\frac{5}{8}$	0.00837(16)	0.0093(2)	0.0093	0.0065(3)	0.0000	0.0000	0.0000
O (16h)	O	1.00	0	0.06598(13)	0.19626(12)	0.01311(14)	0.0168(3)	0.0117(3)	0.00108(2)	0.0000	0.0000	-0.0011(2)
Kolesov et al. (2001) synthetic NRD zircon												
A (4a)	Zr	1.00	0	$\frac{3}{4}$	$\frac{5}{8}$	0.00384(2)	0.00364(6)	0.00364	0.00427(7)	0.00000	0.00000	0.00000
B (4b)	Si	1.00	0	$\frac{3}{4}$	$\frac{1}{8}$	0.00404(4)	0.00402(8)	0.00402	0.0041(1)	0.00000	0.00000	0.00000
O (16h)	O	1.00	0	0.06586(7)	0.19533(7)	0.0066(1)	0.0093(1)	0.0045(1)	0.0058(1)	0.00000	0.00000	-0.0008(1)
Robinson et al. (1971) natural NRD zircon												
A (4a)	Zr	1.00	0	$\frac{3}{4}$	$\frac{5}{8}$	0.0021(1)	0.00212(8)	0.00212	0.0022(1)	0.00000	0.00000	0.00000
B (4b)	Si	1.00	0	$\frac{3}{4}$	$\frac{1}{8}$	0.0037(2)	0.0031(1)	0.00310	0.0049(3)	0.00000	0.00000	0.00000
O (16h)	O	1.00	0	0.0661(1)	0.1953(1)	0.0067(2)	0.0082(1)	0.0069(2)	0.0053(2)	0.00000	0.00000	-0.0000(2)
Ríos et al. (2000) natural RD zircon												
A (4a)	Zr	0.99 (fix)	0	$\frac{3}{4}$	$\frac{5}{8}$	0.00588(5)	0.00600(6)	0.00600	0.00566(7)	0.00000	0.00000	0.00000
	Hf	0.01 (fix)										
B (4b)	Si	1.00	0	$\frac{3}{4}$	$\frac{1}{8}$	0.00557(7)	0.00644(10)	0.00644	0.00382(14)	0.00000	0.00000	0.00000
O (16h)	O	1.00	0	0.06580(8)	0.19545(8)	0.00900(8)	0.01292(18)	0.00716(15)	0.00690(14)	0.00000	0.00000	-0.0010(1)

*RD = radiation damaged, NRD = non-radiation damaged.

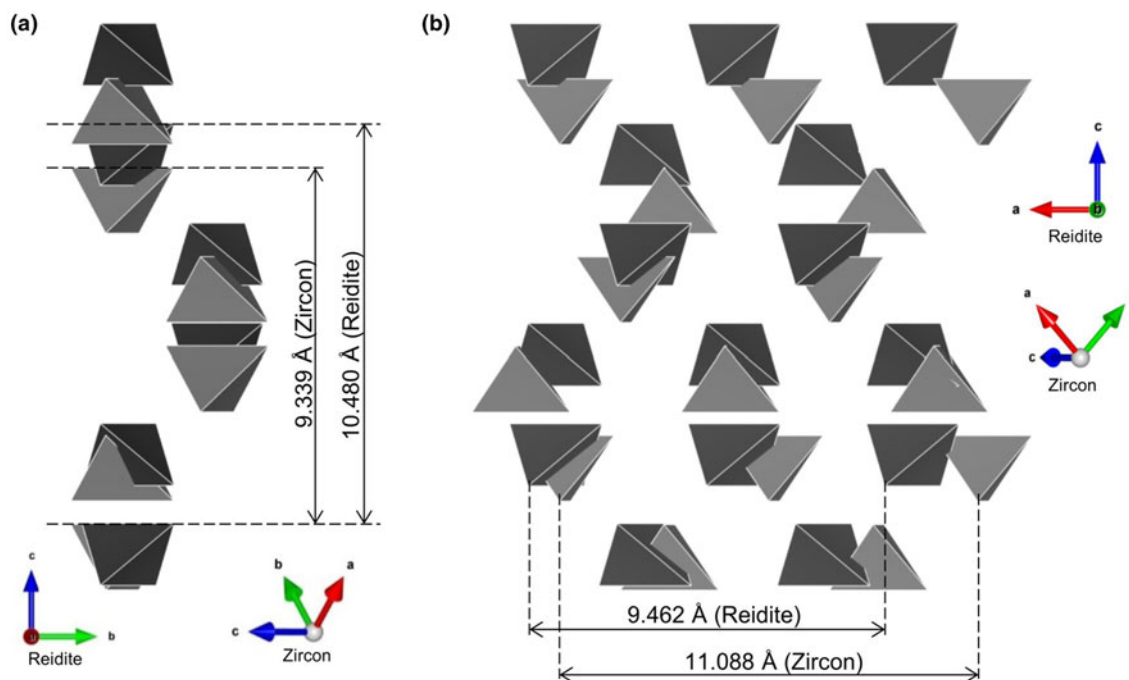
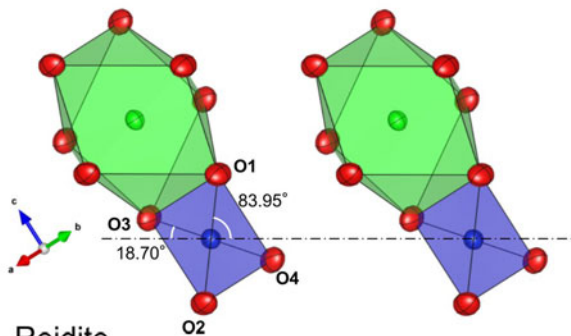


Fig. 2. Comparison of SiO_4 configurations between zircon (Kolesov, *et al.*, 2001) and reidite projected on $(100)_{\text{reidite}}$ (a) and $(010)_{\text{reidite}}$ (b). The grey and black tetrahedra correspond to the SiO_4 of zircon and reidite, respectively.

(a) Zircon



(b) Reidite

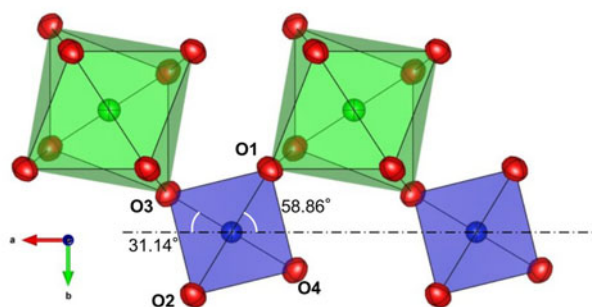


Fig. 3. Twisting of SiO_4 in (a) zircon (Kolesov, *et al.*, 2001) and (b) reidite. Dot-dash lines are the compressed directions of SiO_4 tetrahedra parallel to the a_x axis. Twisting of SiO_4 is represented by angles formed by dot-dash lines and O1–O2 and O3–O4 bonds. The O1–O3 and O2–O4 bonds correspond to the SiO_4 – ZrO_8 shared edge in the zircon structure.

that the structural stability brought by the disappearance of SiO_4 – ZrO_8 shared edges overcomes the instability from enhanced Zr^{4+} – Zr^{4+} repulsions. If this hypothesis is correct, we can conclude that the Si^{4+} – Zr^{4+} repulsion is stronger than the Zr^{4+} – Zr^{4+} repulsion.

Table 4. Comparison of bond distances (Å) and angles (°) for reidite and zircon.

	This study reidite	Kolesov <i>et al.</i> (2001) zircon (synthesised)
SiO_4 tetrahedral		
Si–O ×4	1.6478(8)	1.6225(5)
O1–O2	2.8639(9)	2.7518(8)
O1–O3	2.6000(9)	2.4321(10)
O1–O4	2.6000(9)	2.7518(8)
O1–Si–O2	120.69(7)°	115.99(2)°
O1–Si–O4	104.17(7)°	115.99(2)°
O1–Si–O3	104.17(7)°	97.09(4)°
ZrO_8 dodecahedral		
Zr–O ×4	2.1458(7)	2.1279(5)
Zr–O ×4	2.2593(7)	2.2685(5)
<Zr–O>	2.2025(7)	2.1982(5)

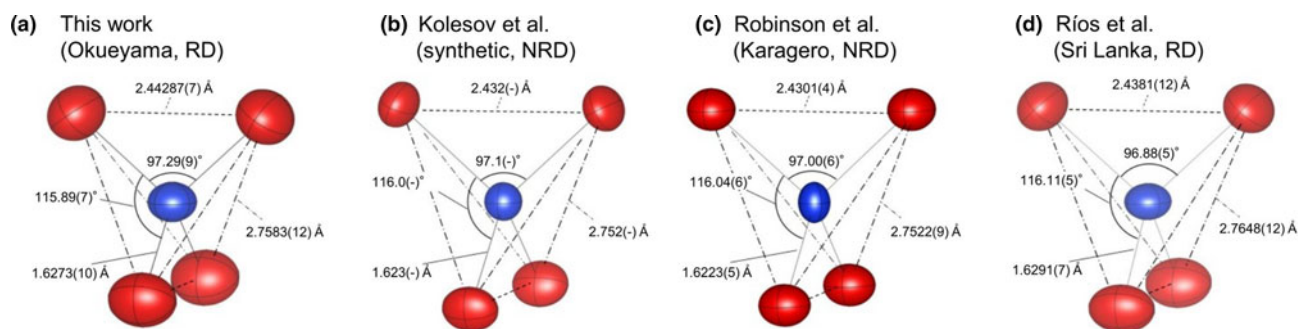
Radiation-damaged natural zircon

To compare with previous studies of natural zircon (Robinson *et al.*, 1971 and Ríos *et al.*, 2000) and synthetic zircon (Kolesov *et al.*, 2001), their structural information is listed in Table 5. Robinson *et al.* (1971) investigated natural non-radiation-damaged zircon from a syenite in Kragerø, Norway, that contained only ~1 wt.% Hf. Ríos *et al.* (2000) used radiation-damaged zircon from Sri Lanka (age 570 ± 20 Ma), whose composition was $\text{Zr}_{0.99}\text{Hf}_{0.01}\text{Si}_{0.95}\text{O}_4$ (1.3 wt.% Hf and <0.01 wt.% U). The lattice parameters of natural zircon are greater than those of synthetic zircon. On the basis of the lattice parameters of synthetic zircon, the ratios $\Delta a/a$ and $\Delta c/c$ of the non-radiation-damaged zircon are 0.047 (15%) and 0.062 (17%), respectively, while those of the Okueyama zircon are 0.591 (3)% and 0.595 (3)%, respectively. The lattice expansion of the radiation-damaged zircon is obviously greater than that of the non-radiation damaged one.

When a zircon is subjected to a stress, the unit cell of the zircon structure elongates along the a_z axis rather than along the c_z axis

Table 5. Comparison of structural parameters for radiation-damaged and non-radiation-damaged zircons.

	This study radiation damaged	Kolesov <i>et al.</i> (2001) synthesised	Robinson <i>et al.</i> (1971) non-radiation damaged	Ríos <i>et al.</i> (2000) radiation damaged
a (Å)	6.64292(18)	6.6039(6)	6.607(1)	6.618(3)
c (Å)	6.0139(2)	5.9783(4)	5.982(1)	6.019(3)
$\Delta a/a$ synthesised	0.591(3)	–	0.047(15)	0.214(45)
$\Delta c/c$ synthesised	0.595(3)	–	0.062(17)	0.681(50)
SiO₄ tetrahedral				
Si–O $\times 4$ (Å)	1.6278(9)	1.6225(5)	1.6223(5)	1.6291(7)
O–O share edge (Å)	2.4449(18)	2.4321(10)	2.4301(4)	2.4381(12)
O–O unshared edge (Å)	2.7587(14)	2.7518(8)	2.7522(9)	2.7648(12)
O–Si–O (1) (°)	97.35(6)	97.09(4)	97.00(6)	96.88(5)
O–Si–O (2) (°)	115.85(4)	115.99(2)	116.04(6)	116.11(5)
Volume (Å ³)	2.142	2.118	2.116	2.141
ZrO₈ dodecahedral				
Zr–O $\times 4$ (Å)	2.1423(9)	2.1279(5)	2.1304(4)	2.1325(10)
Zr–O $\times 4$ (Å)	2.2863(8)	2.2685(5)	2.2688(7)	2.2817(10)
Volume (Å ³)	19.423	19.009	19.049	19.226

**Fig. 4.** SiO₄ tetrahedron in the Okueyama zircon. Dotted and dot-dash lines correspond to the O–O shared edge and unshared edge, respectively. Thermal motions of atoms are drawn as ellipsoids of 99% probability. Note: RD = radiation damaged, NRD = non-radiation damaged.

(Hazen and Finger, 1979). However, the expansion in the Sri Lankan radiation-damaged zircon is greater along the c axis ($\Delta c/c = 0.681(50)\%$) than the a axis ($\Delta a/a = 0.214(45)\%$), where $\Delta a/a$ and $\Delta c/c$ represent the difference in lattice parameter between analysed sample and standard (Kolesov *et al.*, 2001) divided with the lattice parameter of the standard. In studies of ²³⁹Pu-doped zircon and neutron-irradiated zircon, the net lattice expansion by radiation damage is almost equal, within 5.0×10^{18} α -decays/mg (Weber *et al.*, 1998). Murakami *et al.* (1991) suggested that point defects in the early stages of damage accumulation ($<3.0 \times 10^{15}$ α -decays/mg) undergo self-annealing in natural zircon under ambient conditions. We expect that the relaxation of the expansion along the a_z axis is energetically more favourable than that along the c_z axis. The Sri Lankan zircon underwent defect annealing over a long geological time period. The Okueyama zircon is younger and, moreover, the Okueyama granite consists of a single magma chamber, which solidified as a zoned pluton (Takahashi, 1986). Accordingly, we conclude that Okueyama zircons did not undergo thermal recovery of the lattice expansion.

The differences between the Sri Lankan and Okueyama zircons appear in the SiO₄ tetrahedron. The Si–O bond distances in radiation-damaged zircons are significantly longer than in non-radiation-damaged zircons. The increase in Si–O bond distances of radiation-damaged zircon comes from a disordered static displacement of atoms due to the α -decay event. Note that the Si vacancy also contributes to the expansion of the Si–O bond length in radiation-damaged zircon. The O–O shared-edge lengths of radiation-damaged zircon are longer than that of

non-radiation-damaged zircon. In non-radiation-damaged zircon, effects of Si⁴⁺–Zr⁴⁺ repulsions are shielded by the shorter O–O shared-edge length. There are two kinds of O–Si–O bond angle in the zircon structure, as shown in Fig. 4: (1) the O–Si–O angle is with the shared edge between SiO₄ and ZrO₈; and (2) the O–Si–O angle is with the unshared edge. The O–Si–O (1) angle of the Sri Lankan zircon is smaller than that of the Okueyama zircon, which yields a shorter O–O shared-edge length (Table 5). As for the ZrO₈ dodecahedron, the Zr–O bond distance, which links to Si–O bonds in the Sri Lankan zircon, is also shorter than that of the Okueyama zircon. The O–Zr–O (1) angle is with the shared edge between SiO₄ and ZrO₈. The O–Zr–O angle of the Sri Lankan zircon is smaller than that of the Okueyama zircon. The shorter Zr–O bond distances and O–O shared-edge lengths mean that the cation–cation repulsion between SiO₄ and ZrO₈ is suppressed more in zircon studied by Ríos *et al.* (2000) than in the Okueyama zircon. Old Sri Lankan zircons are more structurally relaxed than the young Okueyama zircons. The relaxation of the expansion along the a axis may result from the suppression of the cation–cation repulsion between SiO₄ and ZrO₈.

This can be evaluated by comparing the amplitude of the anisotropic temperature factor as an index of repulsion between cations, as observed in garnet-type (pyrope) and rutile-type (stishovite) structures, where the amplitude decreases in parallel to the direction of repulsion between cations. However, in contrast, it is observed in this work that the amplitude increases in the vertical direction. We observed larger MSD parameters in the Okueyama zircon than in the non-radiation-damaged zircons.

In radiation-damaged zircon, the larger MSD of the atoms contains the contribution of disordered static displacements of atoms due to the α -decay event. Although Zr and Si thermal ellipsoids in non-radiation-damaged zircon are almost spherical ($U^{11} \approx U^{33}$), the thermal ellipsoids in radiation-damaged zircon are obviously flattened ($U^{11} > U^{33}$). The parameters U^{11} and U^{33} of Zr and Si are the MSD along the a_z and c_z axes, respectively. In particular, $U^{11} > U^{33}$ implies Si^{4+} – Zr^{4+} repulsion between SiO_4 and ZrO_8 . Although the MSD parameters of all atoms in the Sri Lankan zircon show the same tendency as in the Okueyama zircon, those values are smaller than those for the Okueyama zircon. From this result, we expect the Si^{4+} – Zr^{4+} repulsion in SiO_4 – ZrO_8 to be weakened by thermal recovery over geological time. The static displacement of Si and Zr from the 8d site due to radiation damage contributes to the flattening of vibration ellipsoids perpendicular to the SiO_4 – ZrO_4 shared edge.

Conclusion

As far as we know, this is the first report on structural data of reidite from single-crystal X-ray diffraction. The mechanism of the zircon–reidite transition can be understood as the twisting and translation of SiO_4 tetrahedra, which accounts for the structural transformation without long-range atomic diffusion. The shared edge between the SiO_4 tetrahedron and ZrO_8 dodecahedron disappears in the transition from the zircon to reidite structure. The disappearance of the SiO_4 – ZrO_8 shared edge yields structural stability according to Pauling's third rule.

We discussed the structural refinement of radiation-damaged Okueyama zircons by comparison with a previous study of synthetic and natural non-radiation-damaged and radiation-damaged zircons. Lattice expansions for the Okueyama zircon are different from those of the radiation-damaged Sri Lankan zircon, which is older. The Sri Lankan zircon underwent defect annealing over a longer geological time period. We conclude that Okueyama zircons did not undergo thermal recovery of the lattice expansion. This thermal relaxation appears especially at atomic distances in the SiO_4 tetrahedron. The Okueyama zircon shows a longer Si–O bond and O–O shared-edge lengths. These structural features imply that the Si^{4+} – Zr^{4+} repulsion in SiO_4 – ZrO_8 are weakened by thermal recovery over geological time.

These structural changes in zircon, induced by pressure or thermal recovery from radiation damage, can be understood by considering the cation–cation repulsion in the SiO_4 – ZrO_8 shared edge. Our study suggests that the cation–cation repulsion in a shared edge should not be ignored and provides fruitful insight into structural stability in edge-sharing compounds.

Supplementary material. To view supplementary material for this article, please visit <https://doi.org/10.1180/mgm.2019.27>

Acknowledgements. Mark Kurban, M.Sc., from Edanz Group (www.edanzediting.com/ac) edited a draft of this manuscript.

References

Akaogi M., Hashimoto S. and Kojitani H. (2018) Thermodynamic properties of ZrSiO_4 zircon and reidite and of cotunnite-type ZrO_2 with application to high-pressure high-temperature phase relations in ZrSiO_4 . *Physics of the Earth and Planetary Interior*, **281**, 1–7.

Brogger W.C. (1893) Amorf. Pp. 742–743 in: *Salmonsens Illustrerede Konversationslexikon*, I. Copenhagen.

Errandonea D. and Manjón F.J. (2008). Pressure effects on the structural and electronic properties of ABX_4 scintillating crystals. *Progress in Materials Science*, **53**, 711–773.

Fukunaga O. and Yamaoka S. (1979) Phase transformation in ABO₄ type compounds under high pressure. *Physical Chemistry of Minerals*, **5**, 167–177.

Glass B.P. and Liu S. (2001) Discovery of high-pressure ZrSiO_4 polymorph in naturally occurring shock-metamorphosed zircons. *Geology*, **29**, 371–373.

Hamberg A. (1914) Die radioaktiven Substanzen und die geologische Forschung. *Geologiska Föreningens Stockholm Förhandlingar*, **36**, 31–96.

Hazen R.M., and Finger L.W. (1979) Crystal structure and compressibility of zircon at high pressure. *American Mineralogist*, **64**, 196–201.

Kolesov B.A., Geiger C.A. and Armbruster T. (2001) The dynamic properties of zircon studied by single-crystal X-ray diffraction and Raman spectroscopy. *European Journal of Mineralogy*, **13**, 939–948.

Kusaba K., Syono Y., Kikuchi M. and Fukuoka K. (1985) Shock behavior of zircon: phase transition to scheelite structure and decomposition. *Earth and Planetary Science Letters*, **72**, 433–439.

Kusaba K., Yagi T., Kikuchi M. and Syono Y. (1986) Structural considerations on the mechanism of the shock-induced zircon-scheelite transition in ZrSiO_4 . *Journal of Physics and Chemistry of Solids*, **47**, 675–679.

Liu L.G. (1979) High-pressure phase transformations in baddeleyite and zircon, with geophysical implications. *Earth and Planetary Science Letters*, **44**, 390–396.

Mashimo T., Nagayama K., and Sawaoka A. (1983) Shock compression of zirconia ZrO_2 and zircon ZrSiO_4 in the pressure range up to 150 GPa. *Physics and Chemistry of Minerals*, **9**, 237–247.

Momma K. and Izumi F. (2008) VESTA: a three-dimensional visualization system for electronic and structural analysis. *Journal of Applied Crystallography*, **41**, 653–658.

Murakami T., Chakoumakos B.C., Ewing R.C., Lumpkin G.R. and Weber W.J. (1991) Alpha-decay event damage in zircon. *American Mineralogist*, **76**, 1510–1532.

Nakatsuka A., Yoshiasa A. and Takeno S. (1995) Site preference of cations and structural variation in $\text{Y}_3\text{Fe}_{5-x}\text{Ga}_x\text{O}_{12}$ ($0 \leq x \leq 5$) solid solutions with garnet structure. *Acta Crystallographica*, **B51**, 737–745.

Nakatsuka A., Yoshiasa A. and Yamanaka T. (1999) Cation distribution and crystal chemistry of $\text{Y}_3\text{Al}_{5-x}\text{Ga}_x\text{O}_{12}$ ($0 < x < 5$) garnet solid solutions. *Acta Crystallographica*, **B55**, 266–272.

Ono S., Funakoshi K., Nakajima Y., Tange Y. and Katsura T. (2004) Phase transition of zircon at high P-T conditions. *Contributions to Mineralogy and Petrology*, **147**, 505–509.

Pauling L. (1929) Pauling rules for ionic structures. *Journal of the American Chemical Society*, **51**, 1010–1026.

Pauling L. (1960) *The Nature of the Chemical Bond*, 3rd edition, p. 93. Cornell University Press, Ithaca, USA.

Reid A.F. and Ringwood A.E. (1969) Newly observed high pressure transformations in Mn_2O_3 , GaAl_2O_4 , and ZrSiO_4 . *Earth and Planetary Science Letters*, **6**, 205–208.

Ríos S., Malcherek T., Salje E.K.H. and Domeneghetti C. (2000) Localized defects in radiation-damaged zircon. *Acta Crystallographica*, **B56**, 947–952.

Robinson K., Gibbs G.V. and Ribbe P.H. (1971) The Structure of zircon: A comparison with garnet. *American Mineralogist*, **56**, 782–790.

Sheldrick G.M. (2015) *SHELXT* – Integrated space-group and crystal-structure determination. *Acta Crystallographica*, **A71**, 3–8.

Shibata K. (1978) Contemporaneity of Tertiary granites in the outer zone of Southwest Japan. *Chishitsu Chosajo Geppo*, **29**, 551–554.

Stubican V.S. and Roy R. (1959) High-pressure scheelite-structure polymorphs of rare-earth vanadates and arsenates. *Zeitschrift für Kristallographie*, **101**, 451–456.

Takahashi M. (1986) Anatomy of a middle Miocene Valles-type caldera cluster: geology of the Okueyama volcano-plutonic complex, southwest Japan. *Journal of Volcanology and Geothermal Research*, **29**, 33–70.

Tange Y. and Takahashi E. (2004) Stability of the high-pressure polymorphs of zircon (ZrSiO_4) in the deep mantle. *Physics of the Earth Planetary Interiors*, **143**, 233–229.

Tokuda M., Yoshiasa A., Mashimo T. and Iishi K. and Nakatsuka A. (2018) The vanadate garnet $\text{Ca}_2\text{NaCd}_2\text{V}_3\text{O}_{12}$: a single-crystal X-ray diffraction study. *Acta Crystallographica*, **C74**, 460–464.

Weber W.J., Ewing R.C., Catlow C.R.A., Díaz de la Rubia T., Hobbs L.W., Kinoshita C., Matzke H., Motta A.T., Nastasi M., Salje E.K.H., Vance E.R. and Zinkle S.J. (1998) Radiation effects in crystalline ceramics for the immobilization of high-level nuclear waste and plutonium. *Journal of Materials Research*, **13**, 1434–1484.